ABUAD Journal of Engineering Research and Development (AJERD)
ISSN (online): 2645-2685; ISSN (print): 2756-6811

Volume 8, Issue 1, 199-214

Morphological and Physico-Mechanical Properties of Nano-Graphene-Oxide from Sugarcane Bagasse for Polymer Composite Reinforcement

Harrison Okechukwu ONOVO[1], Ademola Abiona AGBELEYE[1], Theddeus Tochukwu AKANO[2], Solomon Onaolapo OYEGBAMI[3], Kenechukwu Joshua ORAFUNAM[1], Olugbenga Peter ODEDIRAN[1]

[1]*Department of Metallurgical and Materials Engineering, Faculty of Engineering, University of Lagos 101017, Nigeria*
honovo@unilag.edu.ng/aagbeleye@unilag.edu.ng/joshyham04@gmail.com/gbengaodediran@gmail.com

[2]*Department of Mechanical Engineering, University of Botswana Gaborone, Botswana*
akanott@ub.ac.bw

[3]*Department of Metallurgical and Materials Engineering, College of Engineering, Yaba College of Technology, Lagos Nigeria*
niyioyegbami@gmail.com/solomon.oyegbami@yabatech.edu.ng

Corresponding Author: honovo@unilag.edu.ng, +2348035925649

Date Submitted: 21/02/2025
Date Accepted: 02/04/2025
Date Published: 04/04/2025

Abstract: *Graphene oxide (GO) from biomass offers a sustainable alternative to conventional graphite, yet few studies explore sugarcane bagasse (SB) as a feedstock. This research fills that gap by synthesizing GO from SB termed SBGO and reinforcing epoxy composites with it. Mature SB from Lagos, Nigeria, was processed, oxidized using* $KMnO_4/H_2SO_4$*, and purified with* H_2O_2 *and water washes. SBGO was characterized by BET, TEM, FTIR, UV–Vis, XRD, and Raman spectroscopy. BET analysis revealed a high Langmuir surface area of 579.3 m²/g and mesopores averaging 2.132 nm, favoring uniform dispersion. TEM showed SBGO particles ranging from 5–10 nm up to 30–40 nm agglomerates with irregular, flake-like morphologies. FTIR confirmed successful oxidation via prominent O–H (3200–3600* cm^{-1}*), C=O (1700–1740* cm^{-1}*), and C–O (1000–1300* cm^{-1}*) peaks, while UV–Vis displayed a π–π* peak near 230 nm and an n–π* shoulder around 300 nm, evidencing successful oxidation. XRD patterns exhibited a peak at 25°–30°, indicating partial restoration of the graphitic structure. Raman spectra featured dominant D and G bands, with additional peaks at 568, 1818, 2034, 2208, 2874, and 3050* cm^{-1} *that signal defects and residual biomass features. Polymer composites (PC) with 0–2.0 g SBGO showed increased density (from 1.18 to 1.23 g/cm³) and reduced porosity (from 1.67% to 0.75%). Tensile strength and modulus peaked at 1.5 wt% SBGO, hardness rose from 20.9 to 26.1 VHN, and wear rate dropped by up to 58%. These results confirm that SB-derived GO is an effective, eco-friendly reinforcement that enhances composite strength and durability for high-performance applications.*

Keywords: *Sugarcane Bagasse, Graphene Oxide, Reinforcement Materials, Polymer Composites, Mechanical Properties, Sustainable Materials*

1. INTRODUCTION

Biomass is organic material from plants or animals that can be converted into energy or industrial products, making it essential for a sustainable, circular economy. Major sources comprise agricultural remnants (e.g., corn stalks, sugarcane bagasse, rice husk), forestry residues, industrial organic waste, and municipal solid waste. Unlike fossil fuels which are finite and require millions of years to form, biomass is continuously replenished through photosynthesis [1,2]. With increasing global demands for energy, materials, and food, converting biomass into valuable products is critical for reducing environmental impact and promoting sustainable development [3,4].

Agricultural waste, produced in large quantities due to expanding farming, includes rice husks, wheat straw, maize stalks, and sugarcane bagasse. Often, this waste is burned, decomposed, or landfilled, causing environmental harm [5]. However, modern technologies can convert such waste into valuable products, supporting both environmental sustainability and economic growth while contributing to SDGs 3 and 11. This approach aligns with circular economy principles that favor reuse, recycling, and regeneration to reduce the need for new raw materials and minimize waste [6].

Advances in materials science have driven the development of high-performance polymer composites for aerospace, automotive, and construction applications. GO is a breakthrough nanomaterial that offers superior strength, conductivity, and thermal stability. As a modified form of graphene, GO has a large surface area and oxygen-containing groups that render it hydrophilic and easily dispersible in water [7–9].

Recent studies have explored agricultural waste as an affordable, sustainable source for GO synthesis. SB, the fibrous residue remaining after sugar extraction is a promising candidate. Annually, about 1.84 billion tons of sugarcane stalks are produced worldwide, generating large quantities of SB [10, 11]. Rich in hemicellulose and cellulose, SB could be chemically oxidized to create GO, offering a low-cost raw material while reducing disposal-related environmental issues [12]. This conversion supports sustainable waste management and the circular economy by transforming agricultural residues into high-value materials [13].

GO's unique properties allow it to boost the strength (mechanical), conductivity (thermal), as well as polymer matrices rigidity like epoxy resins, making it ideal for advanced composite materials with improved tensile strength, modulus, and impact resistance [14-16]. However, traditional GO production methods, such as the modified Hummers method, use graphite and hazardous chemicals, leading to high costs and environmental concerns [17]. These drawbacks necessitate the search for sustainable alternatives.

Polymer composites are prized for their high strength-to-weight ratio, versatility, and durability, making them critical for construction, transportation, and electronics [18,19]. However, conventional polymer matrices like epoxy resins are often brittle with low impact resistance. Reinforcing agents such as GO improve interfacial bonding and load transfer, thereby enhancing all-inclusive composite mechanical properties [20]. GO's oxygenated groups facilitate strong interactions with the polymer, ensuring uniform dispersion and effective reinforcement [21,22].

Despite its potential, conventional GO synthesis is energy-intensive, costly, and generates hazardous byproducts due to the use of strong oxidants and graphite precursors [23-25]. While SB has been investigated as a raw material for GO, its application as a reinforcement in polymer composites remains underexplored compared to graphite-derived GO [26].

This research addresses that gap by exploring the synthesis of GO from SB and its use as a polymer composite reinforcing agent. The study employs eco-friendly synthesis methods and characterizes the GO using FTIR, XRD, TEM, BET, and Raman spectroscopy. The reinforced composites are then evaluated for tensile strength, modulus, and wear resistance, with performance compared against conventional composites. This study aims to prevail over the environmental and economic impediments of traditional GO production, supporting sustainable material innovation in line with SDGs 3 and 11 and advancing the circular economy by transforming agricultural waste into top quality products.

2. MATERIALS AND METHODS

2.1 Materials

Materials and chemicals for GO extraction as well as synthesis included dried, ground SB, potassium permanganate (97.5%), ethanol (96%), hydrogen peroxide (30%), distilled water, and sulfuric acid (98%). Additional components were epoxy resin and a polyamine hardener. The chemicals were purchased from a chemical market in Bariga, Lagos. The equipment used comprised a beaker, a three-neck round-bottom flask, and a stirring rod. A magnetic stirrer with a heating plate and a fume hood was also essential. Other apparatus included a filtration funnel, filter paper, a reflux condenser, a ceramic crucible, and a drying oven. Precise measurements were obtained using an analytical balance.

2.2 Materials Collection and Preparation

Sugarcane stalks were sourced from the main market at Mile 12 in Lagos State, Nigeria, and selected for their maturity and lack of damage. They were manually stripped and chopped into smaller segments using a sharp machete. The cut pieces were thoroughly rinsed under running tap water to remove impurities and then pressed to extract the juice. The remaining bagasse was collected, washed, spread on a tray, and sun-dried from 9 am to 4 pm (seven hours per day) every day for fourteen consecutive days. The dried bagasse was ground and sieved through a 145 µm mesh to ensure uniform particle size, then stored in an airtight Ziploc bag for further processing (Figure 1).

2.3 Methods

2.3.1 Synthesis of GO from SB via Oxidation Process

To maintain a consistent temperature, a beaker was placed in an ice bath inside a fume hood. 10 mL of distilled water was added to the beaker, followed by 125 mL of sulfuric acid. The resulting solution was stirred for one minute (Figure 2a). Separately, 25 g of potassium permanganate was melted in 10 mL of distilled water to produce a purple solution (Figure 2b). While stirring continuously and keeping the temperature controlled, the potassium permanganate solution was added gradually to the diluted sulfuric acid. Red sparks appeared during the addition, and the reaction released dark pink fumes along with a highly toxic gas that quickly dissipated in the fume hood. The reaction equation is shown in Equation 1.

$$2\mathrm{KMnO_4} + 3\mathrm{H_2SO_4} \rightarrow \mathrm{K_2SO_4} + 2\mathrm{MnSO_4} + 3\mathrm{H_2O} + 5\mathrm{O_2} \quad (1)$$

Over five minutes, potassium permanganate was slowly added to the mixture while stirring continuously. Ice cubes were intermittently introduced to the ice bath to maintain a low temperature. Next, 8 g of pulverized SB was incorporated, producing yellow sparks along with dark brown fumes and toxic gases. As SB was gradually dispersed, the yellow sparks persisted while the fumes shifted to a yellowish-brown hue. After cooling for 10 minutes, the mixture was carefully transferred to a three-neck round-bottom flask, placed on a hot magnetic stirrer, and connected to a reflux condenser for further processing. All steps were performed in a fume hood for safety.

According to Figure 2c, the mixture is boiled for about 15 minutes at 100 °C using a magnetic stirrer. During this time, its color shifts from dark brown to black. The mixture is then cooled in an ice bath (Figure 2d).

To maintain a consistent temperature, a beaker was placed in an ice bath inside a fume hood. 10 mL of distilled water was added to the beaker, followed by 125 mL of sulfuric acid.

Figure 1: Steps implemented in processing SB: (a) as received stalks, (b) peeled, and (c) cut sugarcane before extracting the wet contents. (d) dried and charred bagasse, and (f) Pulverized bagasse.

The resulting solution was stirred for one minute (Figure 2a). Separately, 25 g of potassium permanganate was melted in 10 mL of distilled water to produce a purple solution (Figure 2b). While stirring continuously and keeping the temperature controlled, the potassium permanganate solution was added gradually to the diluted sulfuric acid. Red sparks appeared during the addition, and the reaction released dark pink fumes along with a highly toxic gas that quickly dissipated in the fume hood. The reaction equation is shown in Equation 1.

To maintain a consistent temperature, a beaker was placed in an ice bath inside a fume hood. 10 mL of distilled

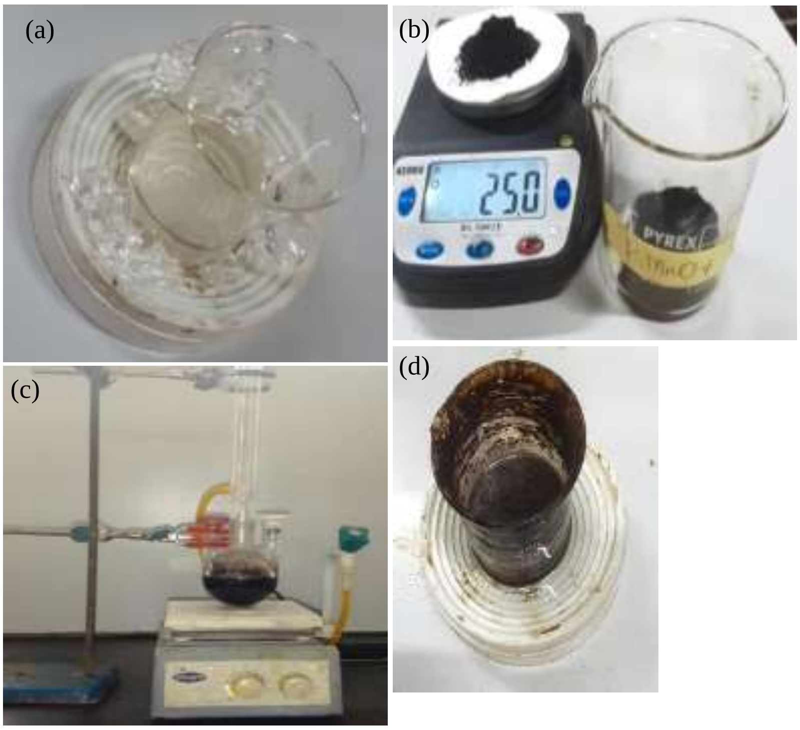

Figure 2: Oxidation processes employed; (a) sulphuric acid in an ice bath, (b) potassium permanganate, (c) heating and refluxing of mixture on a hot magnetic stirrer, and (d) chemical mixture in an ice bath.

water was added to the beaker, followed by 125 mL of sulfuric acid. The resulting solution was stirred for one minute (Figure 2a). Separately, 25 g of potassium permanganate was melted in 10 mL of distilled water to produce a purple solution (Figure 2b). While stirring continuously and keeping the temperature controlled, the potassium permanganate solution was added gradually to the diluted sulfuric acid. Red sparks appeared during the addition, and the reaction released dark pink fumes along with a highly toxic gas that quickly dissipated in the fume hood. The reaction equation is shown in Equation 1.

2.3.1 Dilution, washing, and drying processes *SBGO*

Within the fume hood, the mixture was carefully transferred into a large beaker. Next, 25 mL of hydrogen peroxide was added, followed by 100 mL of distilled water to quench the reaction, as indicated in Equation 2.

$$2KMnO_4 + 3H_2SO_4 + 5H_2O_2 \rightarrow 2MnSO_4 + K_2SO_4 + 8H_2O + 5O_2 \quad (2)$$

Filtration of the mixture was then performed to isolate the solid *SBGO* and the liquid. The solid was purified by washing it several times with distilled water to eliminate residual acid and impurities. These purification steps—including dilution, washing (Figure 3a), and repeated filtration—were repeated until the wash water reached a neutral pH (Figure 3b).

As shown in Figure 4, the purified *SBGO* suspension was carefully poured into a ceramic crucible and dried in an oven at 100 °C, with complete drying achieved within 22 hours.

2.3.2 Production of polymer composite reinforced with *SBGO*

Polymer composites reinforced with *SBGO* (PC-*SBGO*) were produced using five wooden molds, each weighing 100 g. The formulations, labeled PC-*SBGO*: 0, 0.5, 1, 1.5, and 2 (Table 1) were prepared by weighing the appropriate amount of *SBGO* and mixing it with 100 mL of ethanol in five separate beakers. The mixtures were stirred on a magnetic stirrer for one hour to ensure even dispersion. Next, each *SBGO*-ethanol solution was added to the corresponding quantity of epoxy resin while stirring manually. The mixtures were then heated in an oven at 600 °C for 3 hours to evaporate the ethanol. After that, predetermined quantities of hardener were added and thoroughly mixed. Finally, the mixtures were transferred to molds and allowed to cure at ambient temperature for 24 hours.

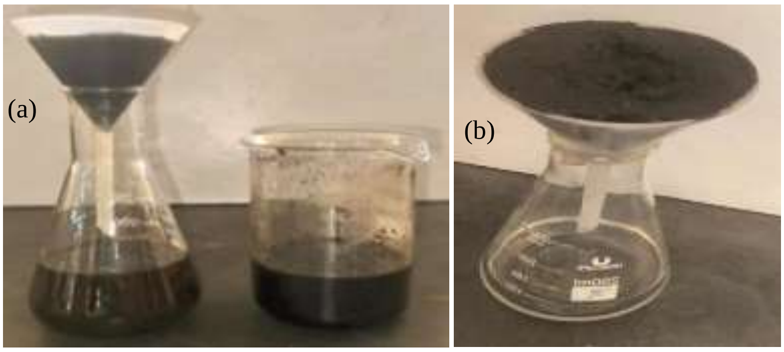

Figure 3: Purification processes adapted; (a) washing progression in beaker, and (b) filtration progression.

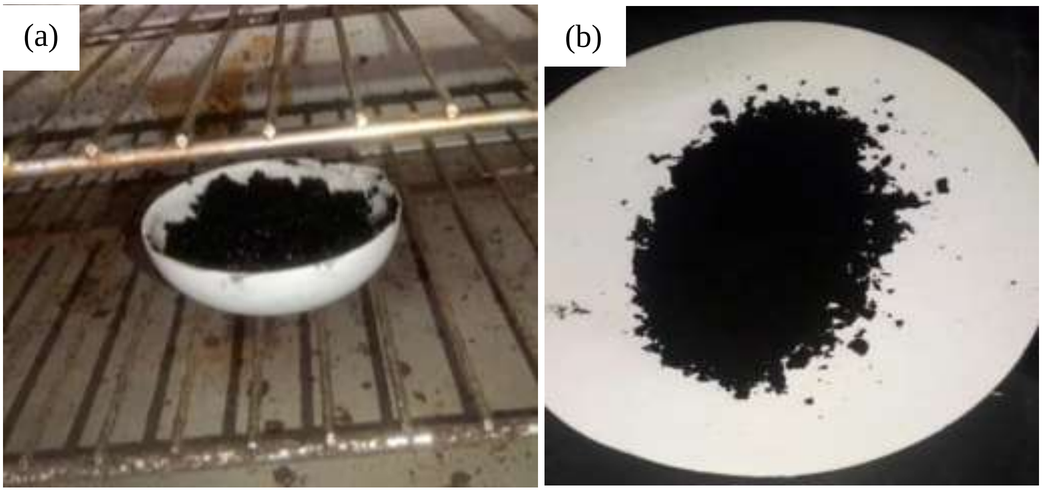

Figure 4: Drying process of GO; (a) wet GO in an oven at 100 °C temperature, and (b) dried GO.

Table 1. Formulations used for the production of PC-*SB*GO

Sample	Epoxy resin (g)	Hardener (g)	GO (g)
PC-*SB*GO:0.0	75.00	25.00	0.00
PC-*SB*GO:0.5	74.75	24.75	0.50
PC-*SB*GO:1.0	74.50	24.50	1.00
PC-*SB*GO:1.5	74.25	24.25	1.50
PC-*SB*GO:2.0	74.00	24.00	2.00

2.3.3 Characterization of *SBGO*

The *SB*GO was characterized using the techniques of TEM (JEM-1400Flash) which produced micrographical and particulate size analysis, and BET analysis described precise surface areas present. FTIR spectroscopy (Shimadzu IRTracer-100) yields specific functional groups/compounds present in *SB*GO. In addition, the UV-Vis Spectrophotometer (LAMBDA 1050+ UV/Vis/NIR (L6020055) spectrum measures the amount of light that *SB*GO can absorb. The X-ray diffraction (Empyrean X-ray Diffraction Alpha-1 system) gives phase details and Raman spectroscopy (OPTOSKY ATR8500) further confirms the presence of *SB*GO phases.

2.3.4 Evaluation of PC-*SBGO* composite density

The density of the PC-*SB*GO was measured in compliance with ASTM D792 standards, to determine the composite's room temperature mass per unit volume. The samples' volume was estimated by $V = \pi r^2 h$, and each sample's weight was assessed via a precision balance of ±0.001 g accuracy level. The density (ρ) was estimated in line with Equation 3.

$$\rho = \text{mass of the sample (g)}/\text{volume of the sample } (cm^3) \quad (3)$$

Where ρ represents the density (g/cm^3). This is to determine the mass per unit volume for the GO-reinforced epoxy composites. In addition, the composite's theoretical density can be evaluated via the formula for the Rule of Mixtures, which calculates the expected density based on the densities and mass fractions of each component in the composite. For the epoxy matrix reinforced with GO, the theoretical density (ρ_c) is calculated with Equation 4.

$$\rho_c = (w_m + w_f) * [(w_m/\rho_m) + (w_f/\rho_f)]^{-1} \quad (4)$$

Where ρ_c, ρ_m and ρ_f are the densities of the composite (theoretical), matrix, and reinforcement, respectively. In addition, w_m *and* w_f are the respective mass fraction of the matrix (epoxy), and filler (GO).

2.3.5 Estimation of PC-*SBGO* composite porosity

The porosity of the PC-*SB*GO composites was measured in compliance with ASTM D2734 standards, to assess the material's structural integrity, and the effects of GO on void content and also to determine the amount of void space within the PC-*SB*GO composites.

2.3.6 Tensile test for PC-*SBGO*

Dog-bone-shaped samples were tested using a 200 kN high-capacity electromechanical universal testing machine with model number WDW-200 following ASTM D3039. The cross-head testing speed of the machine was maintained at 1 mm/min.

2.3.7 Hardness test for PC-*SBGO*

The surface hardness of the SB-derived GO-reinforced epoxy composites was evaluated to determine their resistance to plastic deformation. A microhardness tester (HVN), following ASTM E384, was used with a pointed indenter to measure penetration depth. A 50 gf load was applied for 10 seconds during each test. Multiple indentations were made at various locations on each composite surface to ensure representative values. Hardness readings from twelve points per sample were averaged to account for surface variations. These averages were then compared across samples with different GO weight percentages to assess the effect of GO reinforcement.

2.3.8 Wear rate test for PC-*SBGO*

The wear test evaluated the durability of PC-*SBGO* composites under abrasive conditions according to ASTM G99-17. A pin-on-disc apparatus was employed, where a hardened steel disc rotated against composite pins under loads of 0.2, 0.6, and 1.0 N at speeds of 125 rpm and 250 rpm. The PC-*SBGO* specimens were prepared as rectangular pins (12.5 × 5 × 25 mm) and weighed before testing. Mounted vertically, the pins were pressed against a horizontally rotating disc covered with silicon carbide paper (grit No. 60). With the disc rotating at a 60 mm radius, sliding distances of 141.4 m and 282.8 m were achieved during 3-minute tests at each speed, with a total test time of 10 minutes. After testing, the specimens were cleaned, reweighed, and the weight loss (g), average volume loss (mm^3), and wear rate were calculated using Equations 5–7.

$$\text{Weight loss (g)} = \Delta\text{weight (g)} = \text{final (weight, g)} - \text{initial (weight, g)} \quad (5)$$

$$\text{Volume loss (average) } (\text{mm}^3) = \text{Weight loss (average) (g) }/\text{Density of polyethylene } (\text{g/mm}^3) \quad (6)$$

$$\text{Wear rate } (\text{mm}^3/\text{g}) = \frac{\text{Average volume loss } (\text{mm}^3)}{\text{Density of polyethylene } (\text{g/mm}^3)} * \frac{1}{\text{Load (N)} * \text{Sliding distance (m)}} \tag{7}$$

3. RESULTS AND DISCUSSION

3.1 Characterization of *SBGO* Particulates

3.1.1 BET analysis of *SBGO*

Table 2 presents BET analysis data for *SBGO*, including surface area, pores volume and size from gas adsorption measurements. The Langmuir surface area is 579.3 m²/g, markedly higher than the Single Point BET (136.2 m²/g) and MultiPoint BET (193.2 m²/g) values. This elevated surface area is beneficial for reinforcement, as it increases the contact points between *SBGO* and the polymer matrix, enhancing load transfer and mechanical properties [27]. The BJH cumulative adsorption pore volume is 0.1182 cc/g, while the DR micropore volume is 0.0848 cc/g, suggesting a favorable pore structure that aids in even *SBGO* dispersion within the matrix [28]. A moderate pore volume indicates good porosity, which is vital for maintaining composite integrity and mechanical strength.

The BJH method yielded a pore size (average) of 2.132 nm, confirming the presence of mesopores, whereas the DR method indicated a pore width of 5.749 nm, evidencing both micro- and mesopores [29]. Mesopores facilitate enhanced interaction with the polymer, promoting interlocking and improved composite reinforcement. Additionally, the pore size distribution allows for better polymer infiltration, ensuring effective bonding and stress transfer [30]. The high surface area and optimal pore structure of *SBGO* are expected to significantly enhance polymer composites' tensile strength, modulus, and toughness by ensuring uniform dispersion and superior stress distribution [31].

3.1.2 TEM Analysis of *SBGO*

Figure (5) reveals the morphology and size distribution of *SBGO* particles. It shows a range of particle sizes, from approximately 5-10 nm for smaller particles to 30-40 nm or more for larger agglomerates. These larger entities are likely not individual GO sheets but rather agglomerations, a common characteristic of GO due to strong inter-particle forces comparable to van der Waals forces and π-π stacking [32,33]. The irregular shapes and flake-like appearance of some particles are consistent with the layered graphene structure.

The size variation and prevalent agglomeration are critical considerations for applications. Smaller GO sheets have a higher surface area-to-volume ratio, beneficial for applications like catalysis and sensing [34].

Table 2: BET test result

Test	Surface Area (m²/g)	Pore Volume (cc/g)	Pore Size (nm)
BJH method cumulative adsorption	241.5	0.1182	2.132
DA method	—	—	2.800
DFT method cumulative	540.7	0.0649	2.647
DH method cumulative adsorption	257.2	0.1211	2.132
DR method micropore area	224.0	0.0848	5.749
HK method micropore	—	0.0373	3.675
Langmuir surface area	579.3	—	—
MultiPoint BET	193.2	—	—
SF method micropore	—	0.1075	4.523
Single Point BET	136.2	—	—
t-method external surface area	193.2	—	—

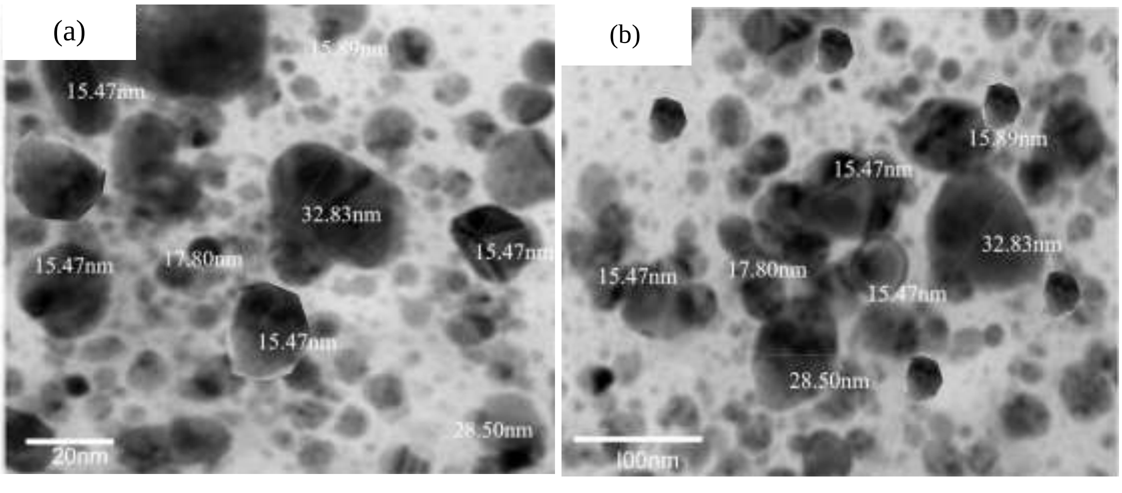

Figure 5: Average particulate sizes of *SBGO*: (a) 20nm, and (b) 100nm.

However, agglomeration can limit the effective use of this surface area by reducing dispersibility and accessibility [35]. This is particularly important because the properties of GO are highly size-dependent. For instance, smaller GO sheets have been shown to exhibit enhanced antibacterial activity compared to larger sheets, due to their ability to more easily penetrate bacterial cell walls [36]. The observed agglomeration could therefore negatively impact the antibacterial performance of this GO sample.

The size and morphology of GO are influenced by the synthesis method and subsequent processing (e.g., oxidation, reduction, sonication) [37]. Controlling these factors is crucial for tailoring GO properties. By way of example, extended sonication can cause larger GO sheets to break down into smaller pieces, thereby increasing the population of smaller-sized particles [38].

3.1.3 FTIR analysis of *SBGO*

Figure 6 presents the FTIR spectrum of *SBGO*, where each peak reflects a specific molecular vibration linked to distinct functional groups. The primary peaks confirm the presence of carbonyl, hydroxyl, and carboxyl functionalities formed during oxidation. *Broad O–H Stretch (3200–3600 cm⁻¹)*: a prominent band in this range represents O–H stretching from adsorbed water and oxygen-based functional groups, verifying the successful oxidation of SB into *SBGO* [39]. *C=O Stretch (1700–1740 cm⁻¹)*: a strong peak here denotes carbonyl (C=O) bonds, often from carboxyl, aldehyde, or ketone groups, signifying the effective oxidation of the biomass precursor [40]. *C=C Skeletal Vibration / O–H Bending (1600–1620 cm⁻¹)*: medium-intensity absorption in this region suggests partial graphitic domains remain, indicating that the aromatic backbone is not fully disrupted [41]. *C–O/C–OH Stretches (1000–1300 cm⁻¹)*: multiple peaks here represent C–O (epoxy or hydroxyl) and alkoxy or carboxy functionalities, confirming abundant oxygen-containing groups in GO [42]. *Minor C–H Stretches (2850–2950 cm⁻¹)*: Weak signals in this zone may arise from residual aliphatic components if the oxidation is not exhaustive [43]. The strong O–H, C=O, and C–O peaks confirm that *SB* was successfully oxidized into *SBGO*. High oxygen content indicates increased hydrophilicity and reactivity, while a peak near 1600 cm^{-1} suggests some retained graphitic structure [44]. These oxygenated groups are essential for interfacial bonding in composites, coatings, or adsorbents, enhancing mechanical and surface properties [45]. The FTIR data in Figure 6 demonstrate the formation of hydroxyl, carbonyl, epoxy, and carboxy functionalities, further confirming the transformation of SB into *SBGO*. This combination of high oxygen content and partial graphitic domains makes *SBGO* a promising reinforcement material for various applications.

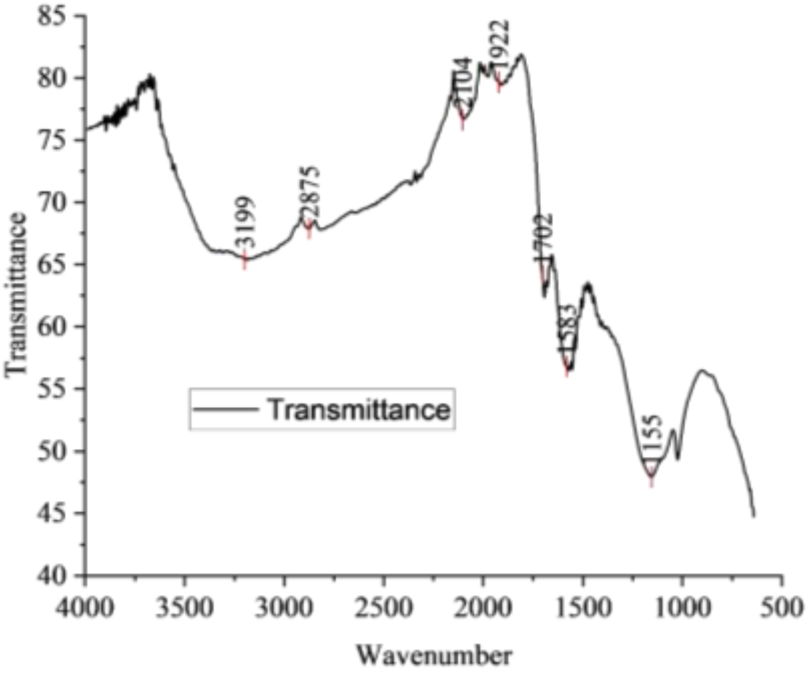

Figure 6: FTIR spectrum of *SBGO*.

3.1.4 Ultra violet analysis of *SBGO*

Figure (7) shows the UV-Vis spectrum of *SBGO* which exhibits two characteristic peaks. (i) A prominent peak around 230 nm. The peak is somewhat broad, and likely the characteristic π-π* transition peak of the aromatic C=C bonds in the graphene structure. This peak's presence indicates the existence of graphitic domains within the GO sheet. The fact that it's not a very sharp peak suggests that the conjugation of the graphene network is disrupted, which is expected in GO due to the extensive oxidation [46]. The exact position of this peak can vary slightly depending on the degree of oxidation and other factors. (ii) Shoulder around 300 nm. This peak in the near-UV/visible region is likely the n-π* transition peak associated with the C=O groups (carbonyl groups). Its lower intensity and broader shape, compared to the π-π* peak, are also typical for GO [46]. This peak indicates the presence of carbonyl, carboxyl, and other oxygen-containing functional groups, which are presented during the oxidation process. The somewhat indistinct nature of this peak might suggest a distribution of different types of carbonyl groups or the influence of other absorbing species in this region.

The presence of both the π-π* and n-π* peaks confirms that the *SBGO* has undergone oxidation, leading to the formation of *SBGO*. The relatively low intensity and broadness of the π-π* peak suggest that the oxidation process has been effective in disrupting the original graphene structure. The presence of the n-π* peak further supports the incorporation of oxygen-containing functional groups. The assertion is consistent with the general understanding of GO synthesis, where strong oxidizing agents are used to introduce oxygen functionalities and disrupt the graphitic structure [47].

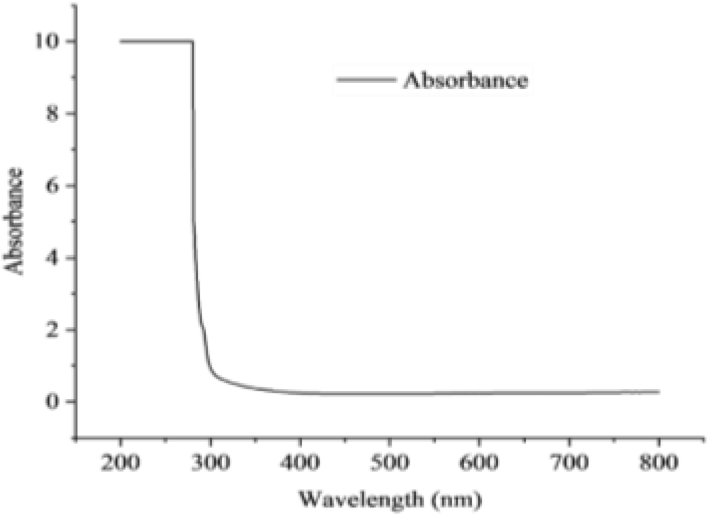

Figure 7: UV-Vis spectrum of *SBGO*.

3.1.5 XRD pattern of *SBGO*

The XRD examination of *SB*GO uncovered a prominent peak located at 2θ = 25°–30°, which resembles the (002) plane of graphitic materials as presented in Figure 8. This peak reflects the interlayer spacing of graphene sheets, a characteristic feature of the layered structure of graphene. The sharpness of this peak indicates a relatively high tendency of crystallinity, which is similar to the deductions of Ikram et al. [48], and Jiříčková et al. [49], where the effective removal of amorphous carbon during the extraction process was shown to enhance crystallinity. Conversely, broader peaks are typically indicative of smaller crystallite sizes and structural defects within graphene sheets, as also highlighted by Eckmann et al., [50].

The absence of a distinct peak near 2θ ≈ 10°, commonly associated with oxidized graphite (GO), suggests successful reduction during the extraction process. This result aligns with observations by Safian et al., [51] and [52], who noted that by removing oxygen-bearing groups, the lessening of *SB*GO facilitates the resurgence of the graphitic structure. The presence of background noise in the XRD pattern likely results from residual amorphous carbon or other non-crystalline organic impurities that were not fully removed during the extraction process. Asif and Saha [53] discussed similar challenges, emphasizing that incomplete pyrolysis or carbonization could lead to such impurities. Optimizing techniques such as thermal annealing or chemical vapor deposition can further improve the crystallinity and reduce amorphous content.

3.1.6 Raman Spectroscopy of *SBGO*

The Raman spectrum (Figure 9) shows two dominant peaks near 1350 cm^{-1} (D-band), and 1580 cm^{-1} (G-band), which indicate structural defects and retained sp^2 domains, respectively [54,55]. In addition to these, smaller peaks appear at 568, 1818, 2034, 2208, 2874, and 3050 cm^{-1}. Such peaks indicate the presence of SB [56, 57]. The 3050 cm^{-1} peak, for instance, corresponds to aromatic C–H stretches, while the 2874 cm^{-1} band may be a D+G combination or a C–H stretch from leftover organic components [58]. The peaks around 1818, 2034, and 2208 cm^{-1} can represent higher-order transitions in partially oxidized carbon [54]. Meanwhile, 568 cm^{-1} may reflect out-of-plane ring deformations linked to residual lignin or cellulose [57]. These minor peaks confirm that *SBGO* retains some biomass-specific features and exhibits complex disorder. This structural diversity can enhance functional group availability and reactivity, benefiting composite applications [59].

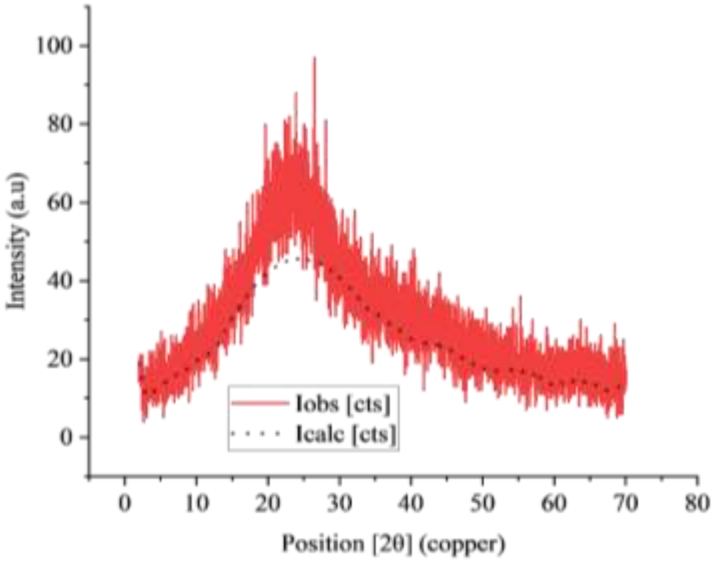

Figure 8: X-ray diffraction analysis showing vibrational modes.

3.2 Characterization of PC-*SBGO* Composites

3.2.1 Estimation of PC-*SBGO* density and porosity

Figure 10a compares the theoretical and measured densities of polymer composites reinforced with *SBGO*. Both densities increase with higher GO content, reflecting the filler's greater density relative to the polymer matrix [60]. However, measured values remain slightly below theoretical ones, likely due to microvoids or incomplete filler dispersion [61]. This small gap suggests effective bonding but indicates some residual porosity [62]. Higher *SBGO* loading raises density, implying improved load transfer and mechanical properties [63].

From the foregoing, the measured density values are roughly 7% lower than the theoretical predictions at lower *SBGO* loadings, narrowing to about 3–5% lower at higher loadings. Nonetheless, both curves show a rising trend with increasing GO content, indicating that the filler's density and its interaction with the polymer matrix play significant roles in the composite's overall density.

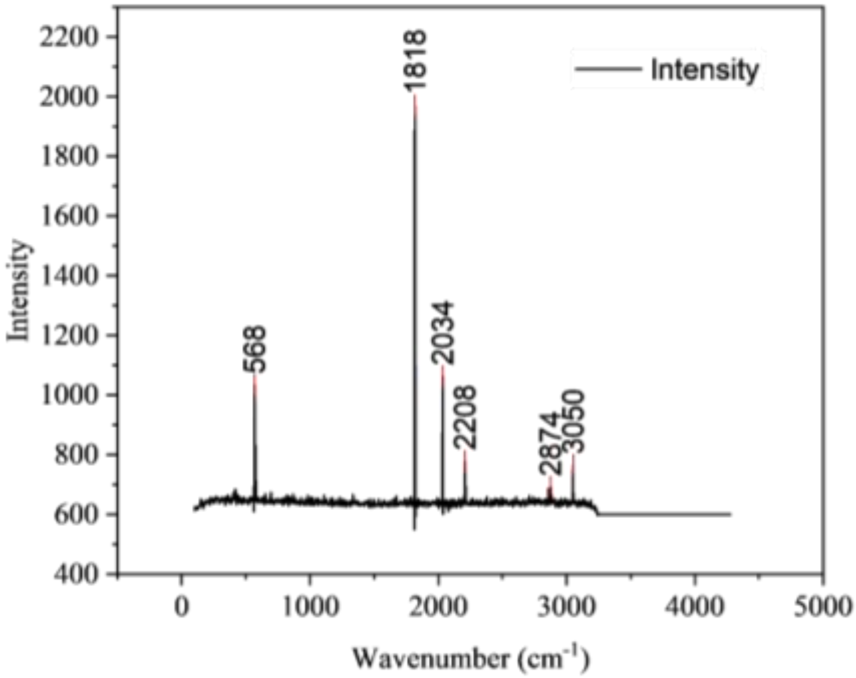

Figure 9: Raman spectrum for *SBGO*.

Based on Figure 10b, porosity decreases as *SBGO* content increases, suggesting fewer voids and improved filler dispersion [60]. The negative slope indicates that added *SBGO* fills microspaces, resulting in a denser composite [61]. Reduced porosity often enhances mechanical properties by improving interfacial bonding and load transfer [62].

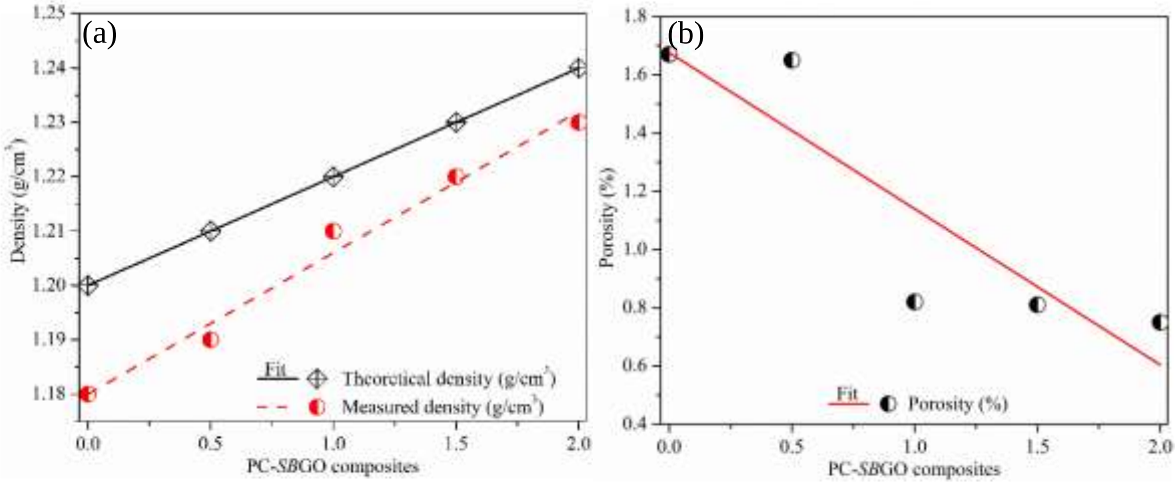

Figure 10: Selected physical properties of PC-*SBGO*, (a) density, and (b) porosity.

3.2.2 PC-*SBGO* Tensile Property

Figure 11 shows stress–strain curves for epoxy composites reinforced with varying *SBGO* content. Pure epoxy (PC-SBGO:0.0) exhibits the highest peak stress (~16 MPa) and moderate strain (~19.6%), reflecting good ductility but limited strength [63]. At 0.5 g *SBGO*, peak stress drops (~7.8 MPa) while strain rises (~48%), suggesting weaker strength but higher ductility, likely due to insufficient filler dispersion [64]. At 1.0 g, peak stress (~8.4 MPa) improves modestly with reduced strain (~32%). The 1.5 g addition boosts peak stress (~12.8 MPa) with moderate strain (~16%), indicating better reinforcement [65]. Further increase to 2.0 g raises peak stress (~14.1 MPa) but offers minimal ductility gain, possibly due to filler agglomeration [66]. Thus, around 1.5 wt% SBGO achieves an optimal balance of strength and ductility, highlighting the importance of proper filler dispersion [67].

3.2.3 PC-*SBGO* Hardness Property

Figure 12 show that *SBGO* reinforcement increases the PC-*SBGO* composite's hardness. The control sample registers 20.9 VHN, a baseline typical of unreinforced polymers [68,69]. With 0.5 g *SBGO*, hardness rises to 22.2 VHN as the filler restricts polymer chain movement [70]. At 1.0 g, hardness increases to 23.2 VHN, indicating improved dispersion. With 1.5 g *SBGO*, the composite reaches 24.5 VHN, reflecting better load transfer and stress distribution [71,72]. The highest hardness, 26.1 VHN, is achieved at 2.0 g *SBGO*, due to cumulative reinforcement and enhanced interfacial bonding [73-75]. The steady hardness increase with more *SBGO* confirms that the filler limits epoxy chain mobility and redistributes applied loads [70,76]. However, excessive *SBGO* may agglomerate, reducing effectiveness [77]. These findings agree with Sharma and Kumar [78], and Abdullah et al. [79], who stress optimal dispersion for superior mechanical performance.

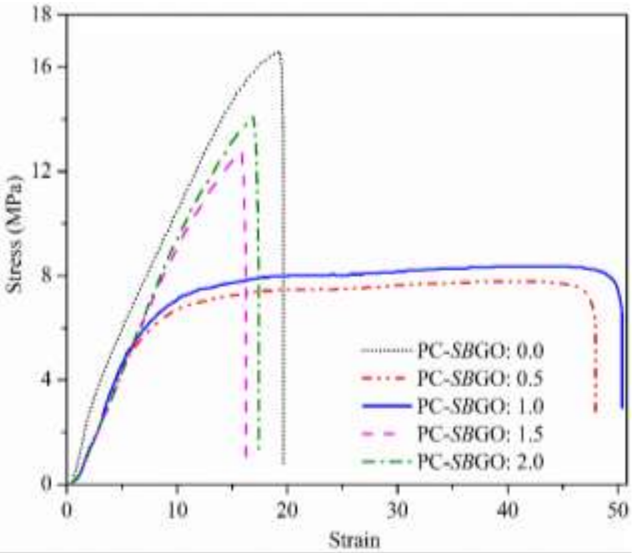

Figure 11: Tensile behaviour of PC-*SB*GO composites.

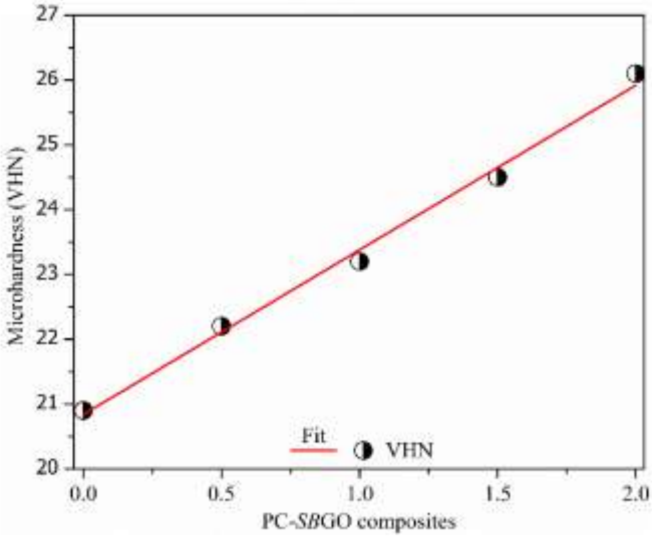

Figure 12: Hardness values of PC-*SB*GO composites.

3.2.4 PC-*SBGO* wear resistance

Figures 13(a) and (b) show that the wear rate decreases as *SBGO* content increases under loads of 0.2, 0.6, and 1.0 N at 150 rpm and 250 rpm. This trend indicates that *SBGO* enhances wear resistance by improving interfacial bonding and providing a lubricating effect [80]. For example, wear rates drop by 50% (from 2.43 to 1.22 mm^3/Nm) at 0.1 N, 54% (from 0.89 to 0.54 mm^3/Nm) at 0.6 N, and 58% (from 0.65 to 0.39 mm^3/Nm) at 1.0 N. The steepest reduction occurs at 0.2 N, suggesting that reinforcement is more effective at lower loads [81]. At higher loads, improved load distribution and *SBGO*-matrix interactions further reduce wear [82]. However, beyond approximately 1.5 wt% *SBGO*, additional filler provides diminishing returns, likely due to agglomeration [83]. The layered structure of *SBGO* also acts as a solid lubricant, decreasing friction and wear [84]. Even at 250 rpm, where friction and heat are greater, the composite still shows significant improvement in wear resistance [85]. These findings confirm that *SBGO* is an effective and economical filler for enhancing the durability of polymer composites.

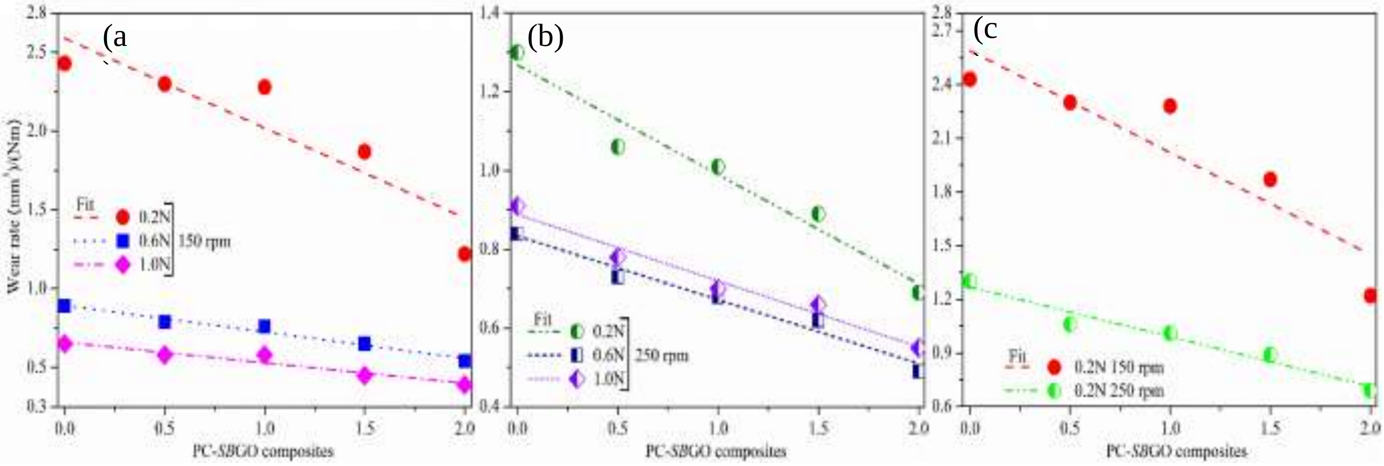

Figure 13: Wear rate of PC-*SBGO* composites at varied loads of 0.2, 0.6, and 1.0 N and constant speed of (a) 150 rpm, (b) 250 rpm, and (c) comparison of 150 and 250 rpm at 0.2N.

Figure 13c further illustrates the wear rate of PC-*SBGO* composites as a function of composite content at two different rotation speeds, 150 rpm and 250 rpm, under a constant load of 0.2 N. The results reveal a clear trend of decreasing wear rate with increasing PC-*SBGO* content across both speeds, indicating that the addition of the graphene oxide reinforcement enhances the wear resistance of the polymer matrix. This aligns with findings that graphene and its derivatives can significantly improve the mechanical properties and wear resistance of polymer composites [86, 87]. Interestingly, the wear rate at 250 rpm is generally lower than that at 150 rpm, suggesting improved wear resistance at the higher speed. This counterintuitive result might be attributed to factors such as frictional heating and the formation of a lubricating film at *a* higher speed, or potentially a shift in the dominant wear mechanism [88]. For instance, higher speeds can induce surface temperature increases, potentially leading to tribochemical reactions that form protective surface layers [89]. The dashed lines represent linear fits to the data, highlighting the overall decrease in wear rate with increasing composite content. The steeper slope observed at 150 rpm suggests a more pronounced initial reduction in wear rate with the addition of PC-*SBGO* at the lower speed, possibly due to a more dominant abrasive wear mechanism at lower speeds which is readily mitigated by the addition of the reinforcement [90]. The scattered data points are typical in wear testing and reflect the inherent complexities of the process. The graph demonstrates the positive impact of surface-brominated graphene oxide reinforcement on the wear performance of polycarbonate composites, with a notable influence of rotation speed on the wear behavior. Further research, such as microscopic analysis of the worn surfaces and friction coefficient measurements, is recommended to fully elucidate the underlying mechanisms and optimize the material's performance for specific applications.

4. CONCLUSION

This research demonstrates that SB can be converted into graphene oxide (GO) through an eco-friendly process, yielding *SBGO* with a high surface area, a mesoporous structure, and abundant oxygenated groups. Characterization confirms that when used as a reinforcement in epoxy composites, *SBGO* significantly improves density, reduces porosity, and enhances key mechanical properties. Tensile testing revealed that pure epoxy exhibited a peak stress of approximately 16 MPa with moderate ductility (strain of ~19.6%). The incorporation of *SBGO* led to notable changes in mechanical behavior: at 0.5 g *SBGO*, the peak stress decreased to around 7.8 MPa while ductility increased (strain ~48%), suggesting that insufficient filler dispersion reduced strength. Increasing the *SBGO* content to 1.0 g slightly improved peak stress to ~8.4 MPa with a strain of ~32%, whereas the addition of 1.5 g produced a peak stress of ~12.8 MPa with reduced strain (~16%), indicating an optimal balance between reinforcement and ductility. At 2.0 g, the peak stress further increased to ~14.1 MPa, though the gains in ductility were minimal, likely due to filler agglomeration.

Hardness measurements corroborated these trends. The control sample registered 20.9 Vickers Hardness Number (VHN), which increased to 22.2 VHN at 0.5 g *SBGO*, 23.2 VHN at 1.0 g, 24.5 VHN at 1.5 g, and reached the highest value of 26.1 VHN at 2.0 g *SBGO*. This steady increase indicates that *SBGO* effectively restricts polymer chain mobility and enhances load transfer.

Wear resistance also improved markedly with *SBGO* reinforcement. Under various loads (0.1, 0.6, and 1.0 N) and rotation speeds (150 and 250 rpm), wear rates decreased significantly: for instance, at 0.1 N, the wear rate dropped by 50% (from 2.43 to 1.22 mm^3/Nm); at 0.6 N, it decreased by 54% (from 0.89 to 0.54 mm^3/Nm); and at 1.0 N, by 58% (from 0.65 to 0.39 mm^3/Nm). These results suggest that *SBGO* enhances wear resistance by improving interfacial bonding and offering a lubricating effect. The data further indicate that the reinforcement effect is more pronounced at lower loads and even at higher speeds (250 rpm), where frictional heating and the formation of a lubricating film may further reduce wear.

Reinforcing epoxy with *SBGO* improves density, reduces porosity, and enhances tensile strength, hardness, and wear resistance. An optimal filler content of approximately 1.5 wt% provides the best balance between strength and ductility, while excessive *SBGO* can lead to agglomeration and diminishing performance gains. These findings underscore the feasibility of utilizing agricultural waste as a low-cost source of GO and confirm the promise of *SBGO* for advanced composite applications. By integrating sustainable material innovation with circular economy principles, and supporting goals such as SDGs 3 and 11, this study paves the way for converting biomass into high-value nanomaterials for greener industries.

ACKNOWLEDGMENT

We extend our profound gratitude to Associate Prof. Henry Ekene Mgbemere, Head of the Department of Metallurgical and Materials Engineering, University of Lagos, for generously providing the laboratory and foundry equipment that made this research possible. His unwavering support and access to vital facilities were instrumental to our success.

REFERENCES

[1] Abhilash, S. V. & Meshram, P. (2021). An overview of chemical processes for synthesis of graphene from waste carbon resources. *Carbon Letters*, 32(3), 653–669. https://doi.org/10.1007/s42823-021-00313-7.

[2] Lee, S., Lee, S. J., Jung, H. S., Kim, A., Ahmed, A. T. A., Inamdar, A. I. & Kim, D. Y. (2017). Ultrathin graphene nanosheets derived from rice husks for sustainable supercapacitor electrodes. *New Journal of Chemistry (1987)*, 41(22), 13792–13797. https://doi.org/10.1039/c7nj03136j

[3] Taiwo, A. E., & Musonge, P. (2024). Valorization of Corn Steep Liquor for Improved Value-added Products: A Review, *Recent Innovations in Chemical Engineering*, 17(1), 26 – 43. DOI: 10.2174/0124055204282376231219095404

[4] Taiwo, A. E., Madzimbamuto, T. F. & Ojumu, T. V. (2020). Development of an Integrated Process for the Production and Recovery of Some Selected Bioproducts from Lignocellulosic Materials. In: Daramola, M., Ayeni, A. (eds) Valorization of Biomass to Value-Added Commodities. *Green Energy and Technology*. *Springer*, *Cham*. https://doi.org/10.1007/978-3-030-38032-8_21

[5] Marinho, B., Ghislandi, M., Tkalya, E., Koning, C. & De, G. (2012). Electrical conductivity of compacts of graphene, multi-wall carbon nanotubes, carbon black, and graphite powder. *Powder Technology*, 221, *351–358.* https://doi.org/10.1016/j.powtec.2012.01.024

[6] Onovo, H. O., Agbeleye, A. A., Akano, T. T., Oludele, D. B., Olawoyin, J. O., & Kentosu, I. S. (2024). Comprehensive Study of Extraction and Applicability of Nanosilicate Particles from Natural Waste for Biopolymer Reinforcement. *Nigerian Journal of Technology (NIJOTECH)*, 43(4), 666-675. https://doi.org/10.4314/njt.v43i4.7

[7] Toto, E.; Laurenzi, S. & Santonicola, M. G. (2022). Recent Trends in Graphene/Polymer Nanocomposites for Sensing Devices: Synthesis and Applications in Environmental and Human Health Monitoring. *Polymers*, 14(5), 1030. https://doi.org/10.3390/polym14051030

[8] Elizalde-Herrera, F. J., Flores-Soto, P. A., Mora-Cortes, L. F., González, F. J., Soria-Arguello, G., Avalos-Belmontes, F., Narro-Céspedes, R. I. & Hoyos, M. (2024). Recent Development of Graphene-Based Composites for Electronics, Energy Storage, and Biomedical Applications: A Review. *Journal of Composites Science*, 8(11), 481. https://doi.org/10.3390/jcs8110481

[9] Worku, A. K. & Ayele, D. W. (2023). Recent advances of graphene-based materials for emerging technologies. *Results in Chemistry*, 5, 100971. https://doi.org/10.1016/j.rechem.2023.100971.

[10] Ungureanu, N., Vlăduț, V. & Biriș, S. -Ș. (2022). Sustainable Valorization of Waste and By-Products from Sugarcane Processing. *Sustainability*, 14(17), 11089. https://doi.org/10.3390/su141711089

[11] Hassan, S., Ngo, T. & Ball, A. S. (2024). Valorisation of Sugarcane Bagasse for the Sustainable Production of Polyhydroxyalkanoates. *Sustainability*, 16(5), 2200. https://doi.org/10.3390/su16052200

[12] Silva, W. C. H., Zafar, M. A., llende, A. S., Jacob, M. V. & Tuladhar, R. (2024). Sustainable Synthesis of Graphene Oxide from Waste Sources: A Comprehensive Review of Methods and Applications. *Mater Circ Econ*, 6(23). https://doi.org/10.1007/s42824-024-00117-w

[13] Maroulas, K. N., Karakotsou, A., Poulopoulos, S. G., Konstantinou, I., Ladomenou, K. & Kyzas, G. Z. (2024). Graphene adsorbents and photocatalysts derived from agricultural wastes: A review, Sustainable Chemistry for the Environment, 8, 100166. https://doi.org/10.1016/j.scenv.2024.100166.

[14] Naveen, C. J. & Gururani, P. (2022). Advances of graphene oxide based nanocomposite materials in the treatment of wastewater containing heavy metal ions and dyes. *Current Research in Green and Sustainable Chemistry*, 5, 100306. https://doi.org/10.1016/j.crgsc.2022.100306.

[15] Heydari, S. F., Shahgholi, M., Karimipour, A., Salehi, M., & Galehdari, S. A. (2024). The effects of graphene oxide nanoparticles on the mechanical and thermal properties of polyurethane/polycaprolactone nanocomposites; a molecular dynamics approach. *Results in Engineering*, 24, 102933. https://doi.org/10.1016/j.rineng.2024.102933.

[16] Onovo, H. O., Agbeleye, A. A., Akano, T. T., Oloyede, O. R., Oyegbami, S. O. & Amoo, E. O. (2024). Characterization of Rice Husk for Graphene Extraction and Metallization. *ABUAD Journal of Engineering Research and Development (AJERD)*, 7(2), 521–531. https://doi.org/10.53982/ajerd.2024.0702.50-j

[17] Ajala, O. J., Tijani, J. O., Bankole, M. T. & Abdulkareem, A. S. (2022). A critical review on graphene oxide nanostructured material: Properties, Synthesis, characterization, and application in water and wastewater treatment. *Environmental Nanotechnology, Monitoring & Management*, 18, 100673. https://doi.org/10.1016/j.enmm.2022.100673.

[18] Rashid, A. B., Haque, M., Islam S. M. M. & Labib, K. M. R. U. (2024). Nanotechnology-enhanced fiber-reinforced polymer composites: Recent advancements on processing techniques and applications, *Heliyon*, 10(2), e24692. https://doi.org/10.1016/j.heliyon.2024.e24692.

[19] Tusher, M. H., Imam A. & Khatun, M. A. (2024). Polymer Composites: Its Processing, Advantages, Properties and Applications. In: Verma, A., Gupta, H.S., Sethi, S.K. (eds) Hybrid *Composite Materials. Springer*, Singapore. https://doi.org/10.1007/978-981-97-2104-7_2

[20] Sriram, G., Arunpandian, M., Dhanabalan, K., Sarojamma, V. R., David, S., Kurkuri, M. D. & Oh, T. H. (2024). Recent Progress Using Graphene Oxide and Its Composites for Supercapacitor Applications: A Review. *Inorganics*, 12(6), 145. https://doi.org/10.3390/inorganics12060145

[21] Itapu, M. B. & Jayatissa, H. A. (2018). A Review in Graphene/Polymer Composites. *Chemical Science International Journal*, 23(3), 1–16. https://doi.org/10.9734/CSJI/2018/41031

[22] Pathak, A. K., Garg, H., Singh, M., Yokozeki, T. & Dhakate, S. R. (2019). Enhanced interfacial properties of graphene oxide incorporated carbon fiber reinforced epoxy nanocomposite: a systematic thermal properties investigation. *J Polym Res*., 26, 23. https://doi.org/10.1007/s10965-018-1668-2

[23] Hummers, W. S. & Offeman, R. E. (1958). Preparation of graphitic oxide. *Journal of the American Chemical Society*, 80(6), 1339-1339. https://doi.org/10.1021/ja01539a017

[24] Joel, E. F. & Lujanienė, G. (2022). Progress in Graphene Oxide Hybrids for Environmental Applications. *Environments*, 9(12), 153. https://doi.org/10.3390/environments9120153

[25] Yusaf, T., Mahamude, A. S. F., Farhana, K., Harun, W. S. W., Kadirgama, K., Ramasamy, D., Kamarulzaman, M. K., Subramonian, S., Hall, S. & Dhahad, H. A. (2022). A Comprehensive Review on Graphene Nanoparticles: Preparation, Properties, and Applications. *Sustainability*, 14(19), 12336. https://doi.org/10.3390/su141912336

[26] Das, P. & Khare, P. (2023). Agricultural waste-derived graphene and its derivatives: opening the way for a sustainable environment, Editor(s): Chaudhery Mustansar Hussain, Ajeet Kumar Srivastav, Chandra Sekhar Tiwary, James M. Tour, In Woodhead Publishing Series in Electronic and Optical Materials, Graphene Extraction from Waste, *Woodhead Publishing*. 213-237, ISBN 9780323909143, https://doi.org/10.1016/B978-0-323-90914-3.00002-4.

[27] Ramesh, M., Rajeshkumar, L., Srinivasan, N., Kumar, D. & Balaji, D. (2022). Influence of filler material on properties of fiber-reinforced polymer composites: A review. *e-Polymers*, 22(1), 898-916. https://doi.org/10.1515/epoly-2022-0080

[28] Guari, Y. (2024). Advanced Porous Nanomaterials: Synthesis, Properties, and Applications. *Nanomaterials*, *14*(19), 1602. https://doi.org/10.3390/nano14191602

[29] Mersellem, K., Bouazza, D., Malpartida, I., Maireles-Torres, P., Boos, A., Demey, H., & Miloudi, H. (2024). Synthesis and Characterization of Mesoporous Materials Functionalized with Phosphinic Acid Ligand and Their Capability to Remove Cd(II). *Molecules*, 29(21), 5199. https://doi.org/10.3390/molecules29215199

[30] Tadayoni, N. S., Dinari, M., Roy, A., & Karimi Abdolmaleki, M. (2024). Recent Advances in Porous Bio-Polymer Composites for the Remediation of Organic Pollutants. *Polymers*, 16(11), 1543. https://doi.org/10.3390/polym16111543

[31] Shahabaz, S. M., Mehrotra, P., Kalita, H., Sharma, S., Naik, N., Noronha, D. J., & Shetty, N. (2023). Effect of Al_2O_3 and SiC Nano-Fillers on the Mechanical Properties of Carbon Fiber-Reinforced Epoxy Hybrid Composites. *Journal of Composites Science*, *7*(4), 133. https://doi.org/10.3390/jcs7040133

[32] Jiříčková, A., Jankovský, O., Sofer, Z., & Sedmidubský, D. (2022). Synthesis and Applications of Graphene Oxide. *Materials (Basel, Switzerland)*, *15*(3), 920. https://doi.org/10.3390/ma15030920

[33] Ren, Yumei & Xu, Yuxi. (2023). Three-dimensional graphene/metal-organic framework composites for electrochemical energy storage and conversion. *Chemical Communications*. 59. 10.1039/D3CC01167D.

[34] Croitoru, A.-M., Moroșan, A., Tihăuan, B., Oprea, O., Motelică, L., Trușcă, R., Nicoară, A. I., Popescu, R.-C., Savu, D., Mihăiescu, D. E., & Ficai, A. (2022). Novel Graphene Oxide/Quercetin and Graphene Oxide/Juglone

Nanostructured Platforms as Effective Drug Delivery Systems with Biomedical Applications. *Nanomaterials*, *12*(11), 1943. https://doi.org/10.3390/nano12111943

[35] Li, F., Jiang, X. Zhao, J. & Zhang, S. (2015). Graphene oxide: A promising Nanomaterial for energy and environmental applications. Nano Energy. 16. 10.1016/j.nanoen.2015.07.014.

[36] Truong, T. T. V., Kumar, S. R., Huang, Y.-T., Chen, D. W., Liu, Y.-K., & Lue, S. J. (2020). Size-Dependent Antibacterial Activity of Silver Nanoparticle-Loaded Graphene Oxide Nanosheets. *Nanomaterials*, *10*(6), 1207. https://doi.org/10.3390/nano10061207

[37] Luceño-Sánchez, J. A., Maties, G., Gonzalez-Arellano, C., & Diez-Pascual, A. M. (2018). Synthesis and Characterization of Graphene Oxide Derivatives via Functionalization Reaction with Hexamethylene Diisocyanate. *Nanomaterials*, *8*(11), 870. https://doi.org/10.3390/nano8110870

[38] Ochigbo, S. S., Obar, A. O., Suleiman, M. A. T. & Kovo, A. S. (2024). Facile Synthesis and Optimization of Graphene Oxide Reduction by Annealing in Hydrazine Vapour in Ambient Air for Potential Application in Perovskite Solar Cells. *Science World Journal*, 19(1), 194-199. https://dx.doi.org/10.4314/swj.v19i1.26

[39] Pattammattel, A., Leppert, V. J., Forman, H. J., & O'Day, P. A., (2019). Surface characterization and chemical speciation of adsorbed iron(iii) on oxidized carbon nanoparticles. *Environmental science. Processes & impacts*, *21*(3), 548–563. https://doi.org/10.1039/c8em00545a

[40] Dedes, G., Karnaouri, A., & Topakas, E. (2020). Novel Routes in Transformation of Lignocellulosic Biomass to Furan Platform Chemicals: From Pretreatment to Enzyme Catalysis. *Catalysts*, *10*(7), 743. https://doi.org/10.3390/catal10070743

[41] Mohan, A. N., B, M. & Panicker, S. (2019). Facile synthesis of graphene-tin oxide nanocomposite derived from agricultural waste for enhanced antibacterial activity against *Pseudomonas aeruginosa*. *Sci Rep*, 9, 4170. https://doi.org/10.1038/s41598-019-40916-9

[42] Olokoba S.W., Mciver F.A. (2024) Synthesis and Characterization of Graphene Oxide from Agricultural Waste: Cocoa pod (Theobroma Cacoa), *J. Mater. Environ. Sci*., 15(9), 1208-1218

[43] Joudeh, N., Linke, D. (2022). Nanoparticle classification, physicochemical properties, characterization, and applications: a comprehensive review for biologists. *J Nanobiotechnol*, 20, 262. https://doi.org/10.1186/s12951-022-01477-8

[44] Shokat, H., & Shrikant, S. M. (2023). Structural, functional and mechanical performance of advanced Graphene-based composite hydrogels, *Results in Chemistry*, 6, 101029. https://doi.org/10.1016/j.rechem.2023.101029.

[45] Shuyan, Z., Wenli, L., Huan, T., Tinglin, H. & Baoshan, X. (2022). Revisit the adsorption of aromatic compounds on graphene oxide: Roles of oxidized debris. *Chemical Engineering Journal*, 450, (1), 137996, https://doi.org/10.1016/j.cej.2022.137996.

[46] Guo, S., Garaj, S., Bianco, A., & Ménard-Moyon, C. (2022). Controlling covalent chemistry on graphene oxide. *Nat Rev Phys*, 4, 247–262. https://doi.org/10.1038/s42254-022-00422-w.

[47] Marcano, D. C., Kosynkin, D. V., Berlin, J. M., Sinitskii, A., Sun, Z., Slesarev, A. S., Alemany, L. B., Lu, W. & Tour, J. M. (2018). *ACS Nano*, 12(2), 2078-2078. DOI: 10.1021/acsnano.8b00128

[48] Ikram, R.; J. Badrul and W. Ahmad. (2020). Advances in synthesis of graphene derivatives using industrial wastes precursors; prospects and challenges. *Journal of Materials Research and Technology*, 9: 15924-15951. 10.1016/j.jmrt.2020.11.043.

[49] Jiříčková, A.; O. Jankovský; Z. Sofer and D. Sedmidubský. (2022). Synthesis and Applications of Graphene Oxide. *Materials*, 15 (3): 920. https://doi.org/10.3390/ma15030920

[50] Eckmann, A.; A. Felten; I. Verzhbitskiy; R. Davey and C. Casiraghi. (2013). Raman study on defective graphene: Effect of the excitation energy, type, and amount of defects. *Physical Review*. 10.1103/PhysRevB.88.035426.

[51] Safian, M. T.; U. S. Haron and M. N. Mohamad Ibrahim. (2020). A review on bio-based graphene derived from biomass wastes, *BioResources*, 15 (4): 9756-9785

[52] Saha, J. K. and Dutta, A. A. (2022). Review of Graphene: Material Synthesis from Biomass Sources. Waste Biomass Valor, 13: 1385–1429. https://doi.org/10.1007/s12649-021-01577-w.

[53] Asif, F. C. and Saha, G. C. (2023). Graphene-like Carbon Structure Synthesis from Biomass Pyrolysis: A Critical Review on Feedstock–Process–Properties Relationship. C, 9 (1): 31. https://doi.org/10.3390/c9010031

[54] Ferrari, A. C., & Basko, D. M. (2013). Raman spectroscopy as a versatile tool for studying graphene. *Nature Nanotechnology*, 8(4), 235–246. https://doi.org/10.1038/nnano.2013.46

[55] Zhu, Y., Murali, S., Cai, W., Li, X., Suk, J. W., Potts, J. R., & Ruoff, R. S. (2010). Graphene and graphene oxide: Synthesis, properties, and applications. Advanced Materials, 22(35), 3906–3924. https://doi.org/10.1002/adma.201001068

[56] Kharlamova, M. V., Kramberger, C., & Chernov, A. I. (2023). Advanced Carbon Nanostructures: Synthesis, Properties, and Applications. *Nanomaterials*, *13*(7), 1268. https://doi.org/10.3390/nano13071268.

[57] Wu, Y., Li, Y., & Zhang, X. (2024). The Future of Graphene: Preparation from Biomass Waste and Sports Applications. *Molecules (Basel, Switzerland)*, *29*(8), 1825. https://doi.org/10.3390/molecules29081825

[58] Zhang, H., Zhou, Y., & Li, C. (2019). *Enhanced interfacial bonding in graphene-based composites*. Composites Science and Technology, 183, 107773.

[59] Joshi, N. N., Narayan, J. and Narayan, R. (2024). Multifunctional carbon-based nanostructures (CBNs) for advanced biomedical applications – a perspective and review. *Mater. Adv.*, *5*(23), 9160-9174. http://dx.doi.org/10.1039/D3MA00636K

[60] Zheng, C., Wei, Z., Rui, Z., Yuqi, T., Kun, H., Fangfang, W., Chao, H., Yong, H., Tao, Y. & Yun, C. (2024). Fabrication and characterization of oxidized starch-xanthan gum composite nanoparticles with efficient emulsifying properties. *Food Chemistry*, 455, 139679. https://doi.org/10.1016/j.foodchem.2024.139679.

[61] Yuqin, X., Yoong, X. P., Yuxin, Y., Ping, Q., Haitao, Z., Sivakumar, M., Tao, W. & Cheng, H. P. (2023). Synthesis and Functionalization of Graphene Materials for Biomedical Applications: Recent Advances, Challenges, and Perspectives. 10(9). 2205292. https://doi.org/10.1002/advs.202205292.

[62] Yoojung, C., Jae, H. K., Hyunseong, S., Seong, D. P. & Hyunseung, Y. (2024). Enhanced interfacial interaction of graphene nanoplatelets/cellulose nanofiber matrix driven by pyranine-based dispersant for efficient thermal managing materials. *Composites Science and Technology*, 255, 110698, https://doi.org/10.1016/j.compscitech.2024.110698.

[63] Pinto, A. M., & Magalhães, F. D. (2021). Graphene-Polymer Composites. *Polymers*, *13*(5), 685. https://doi.org/10.3390/polym13050685

[63] Toplosky, V.J., Walsh, R.P., Tozer, S.W., Motamedi, F. (2000). Mechanical and Thermal Properties of Unreinforced and Reinforced Polyphenylenes at Cryogenic Temperatures. In: Balachandran, U.B., Hartwig, K.T., Gubser, D.U., Bardos, V.A. (eds) Advances in Cryogenic Engineering *Materials*. Springer, Boston, MA. https://doi.org/10.1007/978-1-4615-4293-3_19

[64] Soo, Y. K., Chang, Y. L., Ji-Hun, B., Tae-Yoon, K., & Seung-Hwan, C. (2015). Enhancing the Interfacial Bonding Strength of Carbon/Epoxy Composites Using Silane-Functionalized Graphene Oxides. *Meet. Abstr.* MA2015-01 904. DOI 10.1149/MA2015-01/9/904

[65] Malashin, I., Tynchenko, V., Gantimurov, A., Nelyub, V., & Borodulin, A. (2024). A Multi-Objective Optimization of Neural Networks for Predicting the Physical Properties of Textile Polymer Composite Materials. *Polymers*, *16*(12), 1752. https://doi.org/10.3390/polym16121752

[66] Bheel, N., Mohammed, B. S., Abdulkadir, I., Liew, M. S., & Zawawi, N. A. W. A. (2023). Effects of Graphene Oxide on the Properties of Engineered Cementitious Composites: Multi-Objective Optimization Technique Using RSM. *Buildings*, *13*(8), 2018. https://doi.org/10.3390/buildings13082018

[67] Siraj, S., Al-Marzouqi, A. H., Iqbal, M. Z., & Ahmed, W. (2022). Impact of Micro Silica Filler Particle Size on Mechanical Properties of Polymeric Based Composite Material. *Polymers*, *14*(22), 4830. https://doi.org/10.3390/polym14224830

[68] Joszko, K.; B. Gzik-Zroska; M. Gzik; W. Wolański; M. Ošlejšek; M. Jureczko and Mrowka, M. (2023). Mechanical and tribological properties of epoxy composites reinforced with food-waste fillers. *Journal of Achievements of Materials and Manufacturing Engineering*. 120: 49-58. 10.5604/01.3001.0054.1596.

[69] Kurahatti, R.; A. O. Surendranathan; A. V. R. Kumar; V. Auradi; C. Wadageri and S. Kori. (2014). Mechanical and Tribological Behaviour of Epoxy Reinforced with Nano Al2O3 Particles. Applied Mechanics and Materials. 592-594. 1320-1324. 10.4028/www.scientific.net/AMM.592-594.1320.

[70] Eqra, R.; M. H. Moghim and N. Eqra. (2021). A study on the mechanical properties of graphene oxide/epoxy nanocomposites. Polymers and Polymer Composites, 29 (9): S556-S564. doi:10.1177/09673911211011150

[71] Arun, G. K.; S. Nikhil; R. Kesari; K. Reddy; M. E. S. Kumar and R. Pramod. (2018). Investigation on Mechanical Properties of Graphene Oxide reinforced GFRP. IOP Conference Series: Materials Science and Engineering. 310. 012158. 10.1088/1757-899X/310/1/012158.

[72] Thamilarasan, J.; K. Karthik; B. Sethuraman; V. Ramesh; M. Kumari and S. Bishwakarma. (2023). An Investigation on the Mechanical Properties of Graphene Nanocomposite. 10.1007/978-981-99-2349-6_44.

[73] Khun, N.; H. Zhang; L. Lim and J. Yang. (2015). Mechanical and Tribological Properties of Graphene Modified Epoxy Composites. *KMUTNB International Journal of Applied Science and Technology*. 10.14416/j.ijast.2015.04.001.

[74] Loeffen, A.; D. E. Cree; M. Sabzevari and L. D. Wilson. (2021). Effect of Graphene Oxide as a Reinforcement in a Bio-Epoxy Composite. Journal of Composites Science, 5 (3): 91. https://doi.org/10.3390/jcs5030091

[75] Ropalekar, A.; R. Ghadge and N. Anekar (2023). A review on functionalization methods of graphene oxide for enhancement in mechanical properties of epoxy composites. *Materials Today Proceedings*. 10.1016/j.matpr.2023.09.098.

[76] Bellum, R.; Y. Kuppusamy; C. Durga; C. Venkatesh and G. Sridevi. (2024). Influence of graphene oxide on mechanical and microstructural properties of cement composites. *Research on Engineering Structures and Materials*. 10.17515/resm2024.344me0710rs.

[77] Yuanyuan, F.; P. Bingli; L. Hongyu; Z. Yuxuan; D. Xiaofana and Y. Xinyu (2024). Mechanical and Tribological Behavior of Graphene Oxide Supported Aramid Fiber Reinforced Epoxy Resin. *Journal of Polymer Materials*. 1-10. 10.32604/jpm.2024.055558.

[78] Sharma, R. and Kumar, M. (2020). Mechanical and Tribological Performance of Polymer Composite Materials: A Review. *Journal of Physics: Conference Series*. 1455. 012033. 10.1088/1742-6596/1455/1/012033.

[79] Abdullah, S. and Ansari, M. N. M. (2014). Mechanical properties of graphene oxide (GO)/epoxy composites. *HBRC Journal*. 287. 10.1016/j.hbrcj.2014.06.001.

[80] Soares, P. H. V., De Oliveira, P. N., Viáfara, C. C., Silva, G. G., Amurin, L. G., Da Silva, A. B. (2022). Effect of the reduced graphene oxide on the tribological behavior of UHMWPE/rGO nanocomposites under sliding contact conditions. *Polymer Engineering and Science*, 62(8), 2641-2656. https://doi.org/10.1002/pen.26047

[81] Topal, E., Parmak, E. D. S., Uzunsoy, D., Cakir, O. C. (2017). Investigation of Mechanical Properties of Graphene and Reduced Graphene Oxide Reinforced Epoxy Matrix Composites. *J. Test. Eval.*, 45(4), 1182-1191, https://doi.org/10.1520/JTE20160124

[82] Yazid, M. H., Faris, M. A., Abdullah, M. M. A. B., Nabiałek, M., Rahim, S. Z. A., Salleh, M. A. A. M., Kheimi, M., Sandu, A. V., Rylski, A., & Jeż, B. (2022). Contribution of Interfacial Bonding towards Geopolymers Properties in Geopolymers Reinforced Fibers: A Review. *Materials*, *15*(4), 1496. https://doi.org/10.3390/ma15041496

[83] Qi, C., Zhangxin, G., Feng, C., Gin, B. C., Yongcun. L., Yunbo, L., Jianguo, L. (2022). Effect of GO agglomeration on the mechanical properties of graphene oxide and nylon 66 composites and micromechanical analysis. *Polymer Composites*, 43(11), 8356-8367. https://doi.org/10.1002/pc.27006.

[84] Xue, S., Li, H., Guo, Y., Zhang, B., Li J. & Zeng, X. (2022). Water lubrication of graphene oxide-based materials. *Friction*, 10, 977–1004. https://doi.org/10.1007/s40544-021-0539-8.

[85] Mao, K., Greenwood, D., Ramakrishnan, R., Goodship, V., Shrouti, C., Chetwynd, D., Langlois, P. (2019). The wear resistance improvement of fibre reinforced polymer composite gears, *Wear*, 426–427, Part B, 1033-1039. https://doi.org/10.1016/j.wear.2018.12.043.

[86] Filizzola, A. B., Pereira, J. L. N., dos Santos, P. R., Medeiros, F. da S., do Amparo, S. Z. S., de Vasconcelos, C. K. B. & Silva, G. G. (2024). Enhanced wear resistance of epoxy coatings on steel using graphene oxide. *J Coat Technol Res*, 21, 215–228. https://doi.org/10.1007/s11998-023-00811-5.

[87] Shen, M.-Y., Liao, W.-Y., Wang, T.-Q., & Lai, W.-M. (2021). Characteristics and Mechanical Properties of Graphene Nanoplatelets-Reinforced Epoxy Nanocomposites: Comparison of Different Dispersal Mechanisms. *Sustainability*, 13(4), 1788. https://doi.org/10.3390/su13041788.

[88] Bhushan, B. (2013). Introduction to tribology. John Wiley & Sons. https://doi.org/10.1002/9781118403259.ch1.

[89] Ptak, A., Taciak, P., & Wieleba, W. (2021). Effect of Temperature on the Tribological Properties of Selected Thermoplastic Materials Cooperating with Aluminium Alloy. *Materials*, 14(23), 7318. https://doi.org/10.3390/ma14237318.

[90] Williams, J. A. (2014). Engineering tribology. Chapter 11 - Abrasive, Erosive and Cavitation Wear. Eds: Gwidon W. Stachowiak, Andrew W. Batchelor, Engineering Tribology (4th Ed.), Butterworth-Heinemann, 525-576. https://doi.org/10.1016/B978-0-12-397047-3.00011-4.